ISSN1027-5495. Functional Materials, 32, No.4 (2025), p. 663-671
doi:http://dx.doi.org/10.15407/fm32.04.663

Plasmon-enhanced photocatalysis and antimicrobial activity of $Ag/LaVO_4:Eu^{3+}$ nanoparticle gel for wound healing

V.K. Klochkov[1], O.O. Sedyh[1], G.V. Grygorova[1], N.O. Karpenko[1], P.O. Maksimchuk[1], S.B. Pavlov[2], T.P. Osolodchenko[3], S.L. Yefimova[1]

[1]Institute for Scintillation Materials NAS of Ukraine, 60 Nauky ave., 61072 Kharkiv, Ukraine
[2]Kharkiv National Medical University, 4 Nauky ave., 61022 Kharkiv, Ukraine
[3]I. Mechnikov Institute of Microbiology and Immunology, NAMS of Ukraine, 14-16 Grigory Skovoroda St. 61057 Kharkiv, Ukraine

Receved November 11, 2025

The development of multifunctional biomaterials with both photocatalytic and antimicrobial properties is of great importance for biomedical applications such as wound healing. In this study, we synthesized a hybrid gel containing silver nanoparticles (AgNPs) and europium-doped lanthanum orthovanadate nanoparticles ($LaVO_4:Eu^{3+}$ NPs) embedded in a poly(acrylic acid)–carbomer 940 matrix. Optical and photocatalytic experiments revealed that while $LaVO_4:Eu^{3+}$ NPs alone require high-energy UV excitation (<300 nm) to generate electron–hole pairs, their combination with AgNPs enables efficient plasmon-mediated enhancement under mild UV-A (395 nm) irradiation. This effect is most plausibly attributed to a hot electron injection mechanism, which promotes reactive oxygen species (ROS) formation. Biological assays demonstrated that the $Ag/LaVO_4:Eu^{3+}$ NPs gel completely inhibited the growth of *Staphylococcus aureus* ATCC 25923 after only 10 minutes of UV-A exposure, with no bacterial recovery observed after 4 hours. The interplay of photocatalysis, photothermal activity, and intrinsic antimicrobial properties of AgNPs and $LaVO_4:Eu^{3+}$ contributes to the pronounced and sustained antibacterial effect. Considering the urgent challenge of antibiotic resistance, plasmon-mediated photocatalysis in multifunctional nanocomposite gels provides a powerful alternative strategy for infection control and wound healing applications.

Keywords: plasmon-mediated photocatalysis, $Ag/LaVO_4:Eu^{3+}$ NPs gel, nanoparticles, antimicrobial activity, soft UV-A irradiation

Плазмон-посилений фотокаталіз та антимікробна активність наночастинок $Ag/LaVO_4:Eu^{3+}$, що містяться в гелі для загоєння ран. *В.К. Клочков, О.О. Седих, Г.В. Григорова, Н.О. Карпенко, П.О. Максимчук, С.Б. Павлов, Т.П. Осолодченко, С.Л. Єфімова*

Розробка багатофункціональних біоматеріалів з фотокаталітичними та антимікробними властивостями має велике значення для біомедичних застосувань, таких як загоєння ран. У цьому дослідженні ми синтезували гібридний гель, що містить наночастинки срібла (AgNPs) та наночастинки ортованадату лантану, леговані європієм ($LaVO_4:Eu^{3+}$ NPs), вбудовані в матрицю полі(акрилова кислота)-карбомер 940. Оптичні та фотокаталітичні експерименти показали, що хоча наночастинки $LaVO_4:Eu^{3+}$ самі по собі потребують високоенергетичного УФ-збудження (<300 нм) для генерації електрон-діркових пар, їх поєднання з наночастинками

Ag забезпечує ефективне плазмон-опосередковане посилення під впливом м'якого УФ-А (395 нм) опромінювання. Цей ефект, найімовірніше, пояснюється механізмом інжекції гарячих електронів, який сприяє утворенню активних форм кисню (АФК). Біологічні тестування продемонстрували, що гель, який містить наночастинки Ag/$LaVO_4$:Eu^{3+} повністю пригнічує ріст Staphylococcus aureus ATCC 25923 лише після 10 хвилин впливу УФ-А, при цьому відновлення бактерій не спостерігається через 4 години. Поєднання фотокаталітичної фототермічної активності та власних антимікробних властивостей наночастинок Ag та $LaVO_4$:Eu^{3+} сприяє вираженому та стійкому антибактеріальному ефекту. Враховуючи нагальну проблему стійкості до антибіотиків, плазмон-опосередкований фотокаталіз у багатофункціональних нанокомпозитних гелях забезпечує потужну альтернативну стратегію для контролю інфекцій та загоєння ран.

1. Introduction

Wound healing is a complex and dynamic physiological process involving several overlapping stages: hemostasis, inflammation, proliferation, and the regeneration of skin and subcutaneous tissues. Each of these phases is regulated by intricate cellular and molecular mechanisms and requires a targeted therapeutic approach for optimal recovery [1,2]. In some cases, injuries are accompanied by purulent-inflammatory complications, which pose significant clinical challenges and are often aggravated by persistent infections and impaired wound healing. Modern treatment approaches often rely on the use of various agents (adsorbents, anti-inflammatory drugs, antibiotics, and substances that stimulate the regeneration process), whose actions are targeted at different phases of wound healing [3]. Traditional antibacterial agents that are not based on antibiotics, such as oxidizing agents (e.g., potassium permanganate), can be used only locally and in a limited manner [4]. The main challenge is that active oxidation affects not only bacteria but also wound tissues, thereby complicating the healing process. Moreover, it is important to combine antibacterial and anti-inflammatory effects. The widespread use of antibiotics has sharply exacerbated the problem of bacterial antibiotic resistance and the spread of multidrug-resistant strains [5,6]. Unfortunately, no new classes of antibiotics capable of addressing this issue are currently available. Thus, prolonged inflammation, accompanied by excessive production of reactive oxygen species (ROS) in combination with antibiotic-resistant microbial infections, is a major factor that significantly delays wound healing and requires innovative therapeutic approaches that go beyond conventional methods.

Ultraviolet (UV) irradiation of wounds represents a promising therapeutic approach. In particular, UV-A, with the longest wavelengths (315–400 nm) in the UV spectrum, penetrates human skin more effectively than UV-B (280–315 nm) and UV-C (100–280 nm), reaching the upper layers of the dermis. This deeper penetration, combined with its lower photon energy compared to UV-B and UV-C, suggests a potentially favorable risk-benefit profile for therapeutic applications in living tissues [7,8]. Controlled UV exposure may support wound healing and the restoration of skin homeostasis, partly through its anti-inflammatory and antioxidant effects. This is attributed to UV-A–induced generation of ROS, which can eliminate microorganisms while also acting as signaling molecules.

Low-dose UV-A irradiation can initiate controlled ROS production sufficient to inactivate microorganisms without impairing endogenous antioxidant defense mechanisms, thereby facilitating wound healing [7]. UV-A is particularly attractive due to its lower health risks compared with UV-B and UV-C, as it primarily induces ROS indirectly rather than directly damaging DNA, as UV-C does. This mechanism enables the achievement of therapeutic benefits with minimal side effects [8]. The antimicrobial potential of UV-A can be further enhanced through the use of nanoscale photosensitizers, such as TiO_2 and ZnO nanoparticles (NPs), carbon dots, and silver or copper NPs [9–11]. In this approach, synergistic effects of ROS generation, membrane and DNA damage, and biofilm disruption can be achieved, offering a novel strategy for combating antibiotic-resistant wound infections [9–11].

In the present work, we report on an innovative wound-healing complex in a form of gel containing inorganic redox photoactive nanoparticles of lanthanum orthovanadate doped with Eu^{3+} ions ($LaVO_4$:Eu^{3+}) combined with silver nanoparticles as plasmonic sensitizers, anti-inflammatory and antimicrobial components. The anti-/prooxidant properties of $LnVO_4$:Eu^{3+} NPs (Ln = Gd, Y, La) are well described and attributed to the ability of vanadium ions to exist in multiple oxidation states (V^{3+}, V^{4+}, V^{5+})

within the crystal lattice and participate in diverse redox reactions in cells [12–14]. These unique properties enable $LnVO_4:Eu^{3+}$ NPs to either induce or scavenge ROS, depending on the microenvironmental conditions [13]. Moreover, $LnVO_4:Eu^{3+}$ NPs exhibit a wide range of biological effects, including antibacterial, anti-inflammatory, and wound-healing properties [15-18]. Although these biological processes often involve or depend on oxidative stress, simply listing these diverse effects suggests that the interaction of nanoparticles with biological systems is far more multifaceted than mere ROS scavenging or generation. This indicates that the anti-/pro-oxidant properties of $LnVO_4:Eu^{3+}$ NPs may represent only one component of a broader, more complex profile of biological activity. This profile likely encompasses intricate modulation of cellular signaling pathways, immune responses, and potentially direct antimicrobial actions.

Silver nanoparticles (AgNPs) display potent *in vivo* anti-inflammatory effects via multiple, complementary mechanisms. They suppress the NF-κB signaling pathway—reducing key pro-inflammatory cytokines (IL-1, IL-1ß, IL-6, IL-9, IL-12, IL-18, IFN-γ, TNF-α) through cell membrane penetration, Ag^+ ion release, and ROS generation. This targeted inhibition also lowers C-reactive protein and S-100 B levels, enabling inflammation control without broad immunosuppression [19,20]. Additionally, AgNPs selectively inhibit cyclooxygenase-2 (COX-2), limiting prostaglandin synthesis, reducing leukocyte chemotaxis, and preventing inflammatory exacerbation. Their intrinsic antioxidant activity - scavenging free radicals, reducing oxidative stress biomarkers, and elevating intracellular glutathione - further protects against tissue damage [19,20]. This integrated profile, combining direct molecular inhibition, immune modulation, and oxidative stress reduction, positions AgNPs as versatile candidates for treating diverse inflammatory disorders. Notably, these anti-inflammatory effects complement their well-established antimicrobial activity [20]. A cornerstone of their therapeutic value in wound healing is their broad-spectrum antimicrobial efficacy against Gram-positive and Gram-negative bacteria (e.g., *Staphylococcus aureus*, *Escherichia coli*), fungi (e.g., *Candida albicans*, *Aspergillus niger*), and a wide range of viruses (e.g., HIV, HBV, HSV, influenza virus, SARS-CoV-2) [21,22]. This broad activity prevents and combats infections, a critical factor in preventing chronic wound development. Reported antimicrobial mechanisms include DNA/RNA complex formation, enzyme inactivation and protein denaturation, disruption of ion exchange leading to membrane contraction or rupture, and ROS generation.

Thus, AgNPs and $LnVO_4:Eu^{3+}$ represent promising directions in nanomedicine due to their properties described above. Accordingly, we developed a wound-healing gel containing a combination of AgNPs and $LaVO_4:Eu^{3+}$ NPs. Europium activation of orthovanadate nanoparticles allows a reliable gel identification by characteristic Eu^{3+} luminescent lines in vanadate matrix under UV excitation [23].

2. Experimental section

2.1. Chemicals

Lanthanum chloride $LaCl_3 \cdot 7H_2O$ (99.9%), sodium metavanadate $NaVO_3$ (96%), and disodium EDTA·2Na (99.8%) were purchased from Acros Organics (USA). 1,10-di(3-sulfobutyl)-3,3,3`,3`-tetramethylindodicarbocyanine sodium salt (DiD C4S) was from the dyes collection of Dr. Igor Borovoy (Institute for Scintillation Materials NAS of Ukraine). $AgNO_3$ (99.0%), glycerol (>99.5%), poly(acrylic acid) - carbomer 940 (viscosity 0.5% solution 40 000 – 60 000 cPc) were purchased from Sigma-Aldrich. Sodium tetraborate ($Na_2B_2O_2 \cdot 10\ H_2O$, analytical grade) was from Indiamart (India).

2.2. Synthesis of $LaVO_4:Eu^{3+}$ NPs

$LaVO_4:Eu^{3+}$ NPs in the form of an aqueous colloidal solution were synthesized according to a previously described method [13, 24, 25]. The NPs were stabilized *in situ* during synthesis with sodium EDTA, which imparts a negative surface charge. At the final stage, the colloidal solution was dialyzed against deionized water for 24 h to remove excess ions and organic species, using a dialysis membrane with a molecular weight cut-off of 12 kDa. The resulting colloidal solution remains stable for more than two years without changes in its properties when stored in sealed ampoules under ambient conditions.

2.3. Synthesis of AgNPs

A total of 120 mL of 0.001 M $AgNO_3$ solution was combined with 60 mL of 0.0015 M EDTA solution in a 200 mL beaker and stirred on a magnetic stirrer for 15 min. Subsequently, 8 mL of 0.02 M NaOH solution was added under continuous stirring. The pH of the resulting mixture

was 12–12.5. The beaker was then placed in a water bath equipped with an overhead stirrer and maintained at 90 °C for 18 min. The formation of Ag nanoparticles was monitored by UV–Vis absorption spectroscopy. The reaction mixture developed a light brown coloration, and, upon cooling, exhibited a typical localized surface plasmon resonance (LSPR) peak in the range of 400–430 nm, confirming the formation of silver nanoparticles [26].

2.4. Preparation of a gel containing Ag *and* $LaVO_4:Eu^{3+}$ *NPs*

A total of 46.15 mL of an aqueous $LaVO_4:Eu^{3+}$ NPs suspension (3.9 g/L) was placed in a 300 mL beaker. Carbomer 940 (2.00 g) was added, and the mixture was stirred using a magnetic stirrer and left to hydrate for 24 h at room temperature. The next day, 144.77 mL of an aqueous AgNPs suspension (0.076 g/L) and 20.26 mL of distilled water were added, followed by stirring for 15 min. Subsequently, under vigorous stirring, 12 mL of a 4% (w/v) sodium tetraborate solution ($Na_2B_2O_2$) in glycerol was added. This procedure yielded a homogeneous gel with the following final composition: $LaVO_4:Eu^{3+}$ NPs – 0.8 g/L; AgNPs – 0.049 g/L; $Na_2B_2O_2$ – 2.15 g/L; glycerol – 65.6 g/L; Carbomer – 8.96 g/L.

2.5. Instrumentation and characterization

The size, morphology, and phase composition of the synthesized $LaVO_4:Eu^{3+}$ NPs were analyzed using transmission electron microscopy (TEM) on a JEOL JEM-2100F microscope equipped with a Schottky-type field emission gun, operated at an accelerating voltage of 200 kV. X-ray diffraction (XRD) patterns were obtained using a Siemens D500 X-ray diffractometer (Germany). Zeta potential measurements were performed with a ZetaPALS/BIMAS analyzer (Brookhaven Instruments Corp., USA) in phase analysis light scattering mode. UV–Vis absorption spectra were recorded on a Specord 200 spectrophotometer (Analytik Jena, Germany).

2.6. Measurement of photocatalytic activity of the $Ag/LaVO_4:Eu^{3+}$ *NPs gel under 395 nm irradiation*

A light-emitting diode (LED) flashlight with an emission wavelength of 395 nm was used as a light source. Gel samples were diluted fivefold with distilled water and placed in a quartz cuvette with internal dimensions of 10 × 10 mm. The light source was positioned 3 cm from the sample surface, providing an irradiance of 0.3 W/cm². The photocatalytic activity was evaluated by monitoring the photodegradation of organic dye 1,10-di(3-sulfobutyl)-3,3,3`,3`-tetramethylindodicarbocyanine sodium salt (DiD-C4S) added to the gel, which are readily degraded in the presence of free radicals generated in the medium [27,28]. The dye absorption spectra in the visible spectral range were measured at different time intervals using a Specord 200 spectrophotometer (Analytik Jena, Germany). The intensity of peak at 640 nm, which is assigned to DiD-C3S, was analyzed in the solutions contained the $Ag/LaVO_4:Eu^{3+}$ NPs gel or its components.

2.7. Evaluation of antibacterial activity of $Ag/LaVO_4:Eu^{3+}$ *NPs gel*

The antibacterial effect of the $Ag/LaVO_4:Eu^{3+}$ NPs gel and was evaluated using *Staphylococcus aureus* ATCC 25923 (from the collection of the I. Mechnikov Institute of Microbiology and Immunology of the National Academy of Medical Sciences of Ukraine). The bacterial strain was cultured on nutrient agar at 37 °C for 24 h, and the cell density was adjusted to 0.5 McFarland standard (≈1 × 10^6 CFU/mL) using a Densi-La-Meter (PLIVA-Lachema, Czech Republic; λ = 540 nm). Quartz cuvettes (4 cm × 1 cm) were filled with 1 mL bacterial suspension and 1 mL of the gel. Non-treated samples served as controls. The light source (395 nm LED) was positioned 3 cm from the sample surface, providing an irradiance of 0.3 W/cm². Cuvettes were irradiated for 10 min under the 395 nm LED source, and aliquots were plated on nutrient agar immediately and after 4 h incubation. Colony-forming units (CFUs) were counted to assess antibacterial activity.

3. Results and discussion

3.1. Characteristic of synthesized nanoparticles

The TEM image of synthesized $LaVO_4:Eu^{3+}$ NPs is presented in Fig.1A and reveals rod-like nanoparticles of about 5 x 30 nm size. $LaVO_4:Eu^{3+}$ NPs exhibit a body-centered tetragonal crystal structure, belonging to the I41/amd space group (Fig.1B). The phase identification was confirmed by matching the X-ray diffraction patterns with standard reference data from the PDF-4+ database: card no. 04-006-8778. $LaVO_4:Eu^{3+}$ NPs were found to have a negative surface charge, the ζ-potential was −30.02

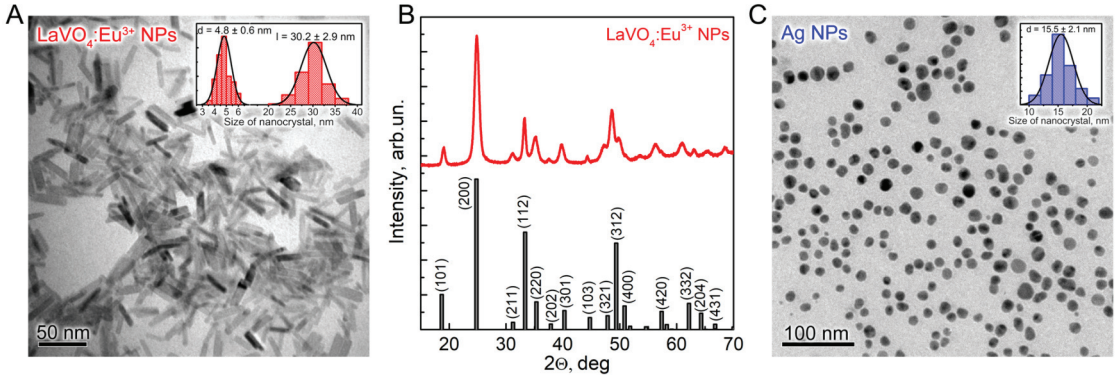

Fig. 1. TEM images with the size distribution diagram of synthesized $LaVO_4:Eu^{3+}$ NPs (A) and Ag NPs (C), XRD pattern of $LaVO_4:Eu^{3+}$ NPs (B).

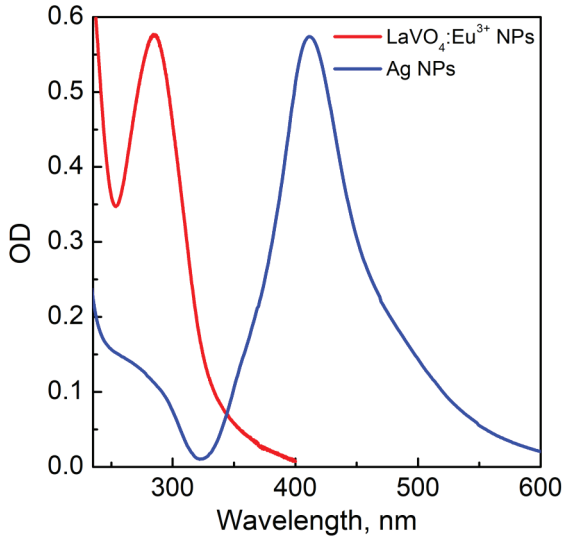

Fig. 2. Absorption spectra of $LaVO_4:Eu^{3+}$ (red curve) and Ag (blue curve) NPs

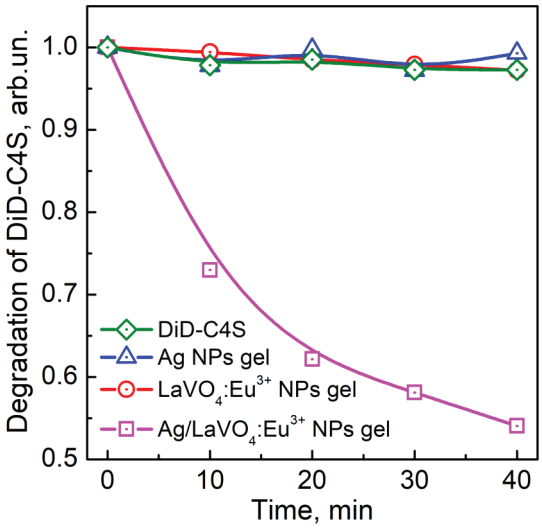

Fig. 3. Time-dependent DiD-C3S dye decomposition in various environment (water, gel containing $Ag/LaVO_4:Eu^{3+}$ NPs and its components) under 395 LED irradiation.

± 0.91 mV. Absorption spectrum of $LaVO_4:Eu^{3+}$ NPs (Fig.2) consists of wide bands in the 260–320 nm spectral range with the maximum centered at 280 nm that corresponds to charge transfer from oxygen ligands to the vanadium atom in the VO_4^{3-} group [29].

Fig.1C represent the TEM image of synthesized AgNPs. The synthesized NPs were of spherical form with the mean size of about 15 nm. The absorption spectrum of AgNPs is shown in Fig.2 and exhibits a characteristic LSPR peak centered at 410 nm.

3.2. Studying photocatalytic activity of the $Ag/LaVO_4:Eu^{3+}$ *gel*

The photocatalytic activity of metal oxide NPs is well established [30]. Upon UV irradiation with photon energy E large then band gap energy E_g ($E>E_g$), metal oxide NPs undergo charge separation, generating conduction-band electrons (e^-) and valence-band holes (h^+). The resulting charge carriers exhibit strong redox potentials, reacting with molecular oxygen and water or hydroxyl ions from photolysis to yield variety of ROS including superoxide ($O_2^{\bullet-}$) and hydroxyl radicals ($\cdot OH$) contributing to a number of photocatalytic effects at the surface of NPs, such as organic dye degradation [30,31]. Photocatalytic properties of $LnVO_4:Eu^{3+}$ (Ln=Gd,Y,La) NPs were studied in our previous works [13,27,28]. The E_g value for $LaVO_4:Eu^{3+}$ NPs was calculated to be 4.12 eV [13] indicating that excitation at wavelengths shorter than 300 nm is required to generate electron–hole pairs (see Fig.2). For example, in [18], a high-pressure mercury lamp providing a light flux of 43 W/cm² was used to observe DID-C3S dye degradation. In contract, irradiation of the gel containing only $LaVO_4:Eu^{3+}$ NPs with a 395 nm LED at a light flux of 0.3 W/cm² did not meet the conditions necessary for DiD-C3S dye degradation via photocatalytic reactions (Fig.3).

Despite the fact that the excitation wavelength of 395 nm corresponds to the LSPR band of AgNPs, no photocatalytic activity was observed in the gel containing only AgNPs (Fig. 3). In contrast, irradiation of the Ag/$LaVO_4$:Eu^{3+} NP gel with a 395 nm LED induced pronounced degradation of the DiD-C3S dye (Fig. 3), whereas no such effect was detected in aqueous suspensions containing both Ag and $LaVO_4$:Eu^{3+} NPs. Furthermore, the effect was absent when the composite was irradiated with visible light from a halogen lamp, even though its luminous flux was an order of magnitude higher than that of the 395 nm LED.

These results indicate that, the UV-A (395 nm) irradiation of the Ag/$LaVO_4$:Eu^{3+} NPs composite, that coincide with LSPR band of AgNPs, enhances the photocatalytic activity of the Ag/$LaVO_4$:Eu^{3+} NPs complex via plasmon-mediated mechanisms, and that the poly(acrylic acid)–carbomer 940 gel matrix provides the spatial confinement necessary for these effects by hosting both types of NPs within its network.

Several mechanisms could contribute to the observed plasmonic photocatalysis upon excitation of the Ag/$LaVO_4$:Eu^{3+} gel within the LSPR band including (i) plasmon-induced resonant energy transfer (PIRET), (ii) electromagnetic local field enhancement (LFE) and (iii) hot electron injection (HEI) [31-34]. Given the absence of spectral overlap between the LSPR band of AgNPs (~410 nm) and the main absorption band of $LaVO_4$:Eu^{3+} NPs (~280 nm), see Fig.2, the contributions of plasmon-induced resonant energy transfer (PIRET) could be excluded [32,33]. In the composite gel, irradiation at the LSPR wavelength induces strong localized electromagnetic fields around AgNPs, which can, in principle, enhance the excitation of nearby semiconductor NPs [33]. For such localized field effects (LFE) to facilitate redox reactions at the NP surface, however, the LSPR wavelength must overlap with the semiconductor band gap. Since no such overlap occurs in our system, LFE cannot efficiently drive photocatalytic processes. Nevertheless, Eu^{3+} has direct excitation band near 395 nm, corresponding to $^7F_0 \rightarrow {}^5L_6$ transition [36,37]. This spectral proximity to the AgNPs' LSPR suggests that LFE could instead enhance Eu^{3+} luminescence. However, the overall efficiency of this process is inherently low, because the $4f^n$–$4f^n$ intra-configurational transitions of Eu^{3+} are only weakly allowed [36,37].

Upon 395 nm excitation, the plasmonic oscillations of AgNPs decay non-radiatively, generating high-energy ("hot") electrons [32,34]. If these electrons possess sufficient energy to overcome the Schottky barrier at the Ag/$LaVO_4$:Eu^{3+} NPs interface, they can be injected into the conduction band of $LaVO_4$:Eu^{3+} NPs. The injected electrons could participate in redox reactions, enhancing the formation of ROS and promoting DiD-C3S dye degradation (Fig.3).

Let us estimate the possibility for HEI in the Ag/$LaVO_4$:Eu^{3+} interface. Photon energy at 395 nm: $h\nu = 3.14eV$. The Fermi level (E_F) of silver is commonly referenced based on its work function, typically around - 4.26 eV below the vacuum level. Maximum energy of a hot electron (in the simplest model) [34]:

$$E_{hot}^{max} \approx E_F + h\nu \approx -4.26 + 3.14 = \\ = -1.12eV(vacuum).$$

Conduction band minimum (CBM) of $LaVO_4$:Eu^{3+} NPs: $E_{CBM} = -$ 3.48 eV *(vacuum)* [13]. Thus, −1.12eV > −3.48eV indicating that hot electrons possess a significant excess energy (~2.36 eV) relative to the CBM and are energetically capable of injection into the conduction band of $LaVO_4$:Eu^{3+} NPs.

Another useful parameter is the Schottky barrier (Φ_b) between the Ag E_F and the $LaVO_4$:Eu^{3+} NPs CBM: $\Phi_b = E_{CBM} - E_F(Ag) = 0.78eV$. This means that for electron injection to occur, a hot electron must carry at least ≥ 0.78 eV of excess energy. Since excitation at $h\nu = 3.14eV$ provides sufficient energy, hot-electron injection is energetically feasible.

Thus, the most plausible mechanism underlying the plasmon–mediated photocatalytic enhancement in the Ag/$LaVO_4$:Eu^{3+} NPs composite seems to be the hot electron injection. The carbomer gel matrix likely facilitates this process by maintaining close spatial proximity and stable contact between the Ag and $LaVO_4$:Eu^{3+} NPs, which is essential for efficient charge transfer. The concept of "plasmonic photocatalysts" was first introduced by Awazu and co-authors in 2008 [38] and since then, the plasmon-mediated enhancement of semiconductor NPs catalytic properties has been widely demonstrated in various composites, such as Ag/TiO_2, Au/TiO_2, Au/ZnO, Au/CeO_2, Ag/Cu_2O and others [32-34]. However, Ag/$LaVO_4$:Eu^{3+} NPs embedded in a gel matrix is reported for the first time.

It should be noted that, in addition to plasmon-mediated photocatalysis, other mechanisms associated with NPs surface reactions under the UV-A (395 nm) irradiation could be

possible and will be the subject of our further studies. The irradiation of AgNPs within the LSPR band can also induce photothermal effects and the combined action of hot carriers, ROS generation, and localized heating, as well as antimicrobial activity of both AgNPs and $LaVO_4:Eu^{3+}$ NPs, thereby endowing the $Ag/LaVO_4:Eu^{3+}$ NPs composite with exceptional antimicrobial and anti-inflammatory properties.

3.3. Evaluation of antibacterial activity of the $Ag/LaVO_4:Eu^{3+}$ NPs gel

The antimicrobial activity of the $Ag/LaVO_4:Eu^{3+}$ NPs gel was tested with *Staphylococcus aureus* ATCC 25923 bacterial strain, which is a gold standard to test antimicrobial preservatives, and bacterial resistance of test substances. (Fig.4). As shown in Fig.4, upon UV-A irradiation (395 nm LED) of the samples without the $Ag/LaVO_4:Eu^{3+}$ NPs gel for 10 minutes (+UV group), no immediate difference in bacterial colony counts was observed compared with the control (10^4 colonies). However, after 4 hours, the number of colonies decreased substantially to 10^2, suggesting that 395 nm light alone exerts a delayed bacteriostatic effect. In the presence of the $Ag/LaVO_4:Eu^{3+}$ NPs gel without an irradiation (+gel group), bacterial growth remained unaffected after 10 minutes, but a pronounced reduction was observed 4 hours later (down to 3–4 colonies). This delayed effect is most likely related to the intrinsic antimicrobial activity of Ag [19,20] and $LaVO_4:Eu^{3+}$ [15] described above and UV-A light irradiation (Fig.4). Most notably, when samples containing the $Ag/LaVO_4:Eu^{3+}$ NPs gel (+gel+UV group) were irradiated with 395 nm light, complete inhibition of bacterial growth was achieved after just 10 minutes, and no regrowth was detected even 4 hours post-irradiation. These findings strongly suggest that the enhanced antibacterial effect arises from the synergistic action of UV-A light and the $Ag/LaVO_4:Eu^{3+}$ NPs composite. In particular, plasmon-mediated ROS generation enhancement together with possible photothermal and intrinsic antimicrobial effects appear to play a decisive role in producing long-lasting antibacterial activity.

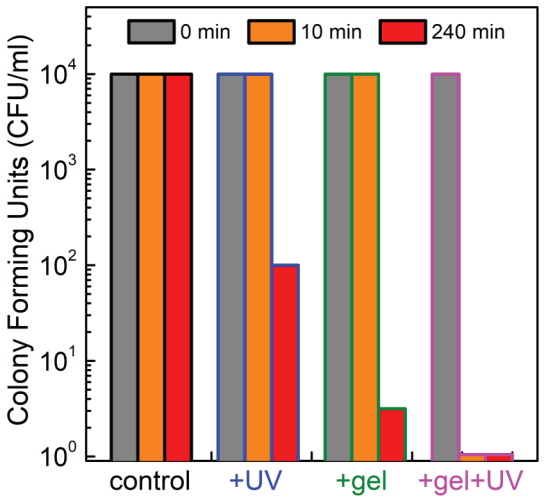

Fig. 4. Growth inhibition of *Staphylococcus aureus ATCC 25923* under different treatment conditions: control – untreated bacterial culture; +UV – exposure to UV-A light (395 nm LED); +gel – treatment with $Ag/LaVO_4:Eu^{3+}$ NPs gel; +gel+UV combined treatment with $Ag/LaVO_4:Eu^{3+}$ NPs gel and UV-A light.

4. Conclusion

In this study, we developed a hybrid gel composed of Ag and $LaVO_4:Eu^{3+}$ nanoparticles embedded within a poly(acrylic acid)–carbomer 940 matrix and evaluated its photocatalytic and antimicrobial performance. While $LaVO_4:Eu^{3+}$ nanoparticles alone require high-energy UV excitation to initiate photocatalysis, the incorporation of AgNPs enables plasmon-assisted enhancement, most likely via a hot electron injection mechanism, resulting in efficient ROS generation under mild UV-A (395 nm) irradiation. The contribution of enhanced photocatalytic activity, photothermal effects, and the intrinsic antimicrobial properties of AgNPs and $LaVO_4:Eu^{3+}$ NPs appears to be crucial for achieving a strong and long-lasting antibacterial response under these soft illumination conditions. Notably, the $Ag/LaVO_4:Eu^{3+}$ NPs gel completely inhibited the growth of *Staphylococcus aureus* ATCC 25923 after short UV-A (395 nm) exposure, with no bacterial recovery observed even after 4 hours. In light of the global challenge of antibiotic resistance, the $Ag/LaVO_4:Eu^{3+}$ NPs gel leveraging plasmon-mediated photocatalysis offer a powerful alternative strategy for infection control, with strong potential to be extended toward broader biomedical applications, including advanced wound healing and tissue regeneration.

Acknowledgments. This work was supported by the National Research Foundation of Ukraine [grant number 2023.04/0006]. S.P. and T.O. thank the Ministry of Health of Ukraine for supporting antibacterial activity research [Project № 0124U000579]. The authors used ChatGPT (OpenAI) to assist with English editing.

References

1. S.L. Sim, S. Kumari, S. Kaur, K. Khosrotehrani, Macrophages in skin wounds: functions and therapeutic potential, Biomolecules 12 (2022) 11. https://doi.org/10.3390/biom12111604
2. Y.H. Almadani, J. Vorstenbosch, P.G. Davison, A.M. Murphy, Wound Healing: A Comprehensive Review, Semin. Plast. Surg. 35 (2021) 141–144. https://doi.org/10.1055/s-0041-1731681
3. C.K. Sen, G.M. Gordillo, S. Roy, R. Kirsner, L. Lambert, T.K. Hunt, F. Gottrup, G.C. Gurtner, M.T. Longaker, Human skin wounds: A major and snowballing threat to public health and the economy, Wound Repair Regen. 17 (2009) 763–771. https://doi.org/10.1111/j.1524-475X.2009.00543.x
4. I. Delgado-Enciso, V.M. Madrigal-Perez, A. Lara-Esqueda, M.G. Diaz-Sanchez, J. Guzman-Esquive, L.E. Rosas-Vizcaino, et al., Topical 5% potassium permanganate solution accelerates the healing process in chronic diabetic foot ulcers, Biomed. Rep. 8 (2018) 156–159. https://doi.org/10.3892/br.2018.1038
5. P. Rajput, K.S. Nahar, K.M. Rahman, Evaluation of antibiotic resistance mechanisms in gram-positive bacteria, Antibiotics (Basel) 13 (2024) 1197. https://doi.org/10.3390/antibiotics13121197
6. P. Bhowmik, B. Modi, P. Roy, A. Chowdhury, Strategies to combat Gram-negative bacterial resistance to conventional antibacterial drugs: A review, Osong Public Health Res. Perspect. 14 (2023) 333–346. https://doi.org/10.24171/j.phrp.2022.0323
7. A. Gupta, P. Avci, T. Dai, Y.-Y. Huang, M.R. Hamblin, Ultraviolet radiation in wound care: sterilization and stimulation, Adv. Wound Care 2 (2013) 422–437. https://doi.org/10.1089/wound.2012.0406
8. J. Inkaran, A. Tenn, A. Martyniuk, F. Farrokhyar, A. Cenic, Does UV light as an adjunct to conventional treatment improve healing and reduce infection in wounds? A systematic review, Adv. Skin Wound Care 34 (2021) 1–6. https://doi.org/10.1097/01.ASW.0000734031.18241.c3
9. A.-G. Niculescu, A.M. Grumezescu, Photodynamic therapy—an up-to-date review, Appl. Sci. 11 (2021) 3626. https://doi.org/10.3390/app11083626
10. T. Sangnim, V. Puri, D. Dheer, D.N. Venkatesh, K. Huanbutta, A. Sharma, Nanomaterials in the wound healing process: new insights and advancements, Pharmaceutics 16 (2024) 300. https://doi.org/10.3390/pharmaceutics16020300
11. H.F. Hetta, Y.N. Ramadan, A.I. Al-Harbi, E.A. Ahmed, B. Battah, N.H. Abd Ellah, S. Zanetti, M.G. Donadu, Nanotechnology as a promising approach to combat multidrug resistant bacteria: a comprehensive review and future perspectives, Biomedicines 11 (2023) 413. https://doi.org/10.3390/biomedicines11020413
12. A. Onishchenko, V. Myasoedov, S. Yefimova, O. Nakonechna, V. Prokopyuk, D. Butov, U. Kökbaş, V. Klochko, P. Maksimchuk, N. Kavok, A. Tkachenko, UV light-activated $GdYVO_4:Eu^{3+}$ nanoparticles induce reactive oxygen species generation in leukocytes without affecting erythrocytes in vitro, Biol. Trace Elem. Res. (2021). https://doi.org/10.1007/s12011-021-02867-z
13. S.L. Yefimova, P.O. Maksimchuk, V. Seminko, N.S. Kavok, V.K. Klochkov, K.A. Hubenko, A.V. Sorokin, I.Y. Kurilchenko, Y.V. Malyukin, Janus-faced redox activity of $LnVO_4:Eu^{3+}$ (Ln = Gd, Y, La) nanoparticles, J. Phys. Chem. C 123 (2019) 15323–15329. https://doi.org/10.1021/acs.jpcc.9b02345
14. Y. Kot, V. Klochkov, V. Prokopiuk, O. Sedyh, G. Grygorova, N. Karpenko, K. Kot, A. Onishchenko, S. Yefimova, A. Tkachenko, $GdVO_4:Eu^{3+}$ and $LaVO_4:Eu^{3+}$ Nanoparticles exacerbate oxidative stress in L 929 cells: potential implications for cancer therapy, Int. J. Mol. Sci. 25 (2024) 11687. https://doi.org/10.3390/ijms252111687
15. S. Gonca, S. Yefimova, N. Dizge, A. Tkachenko, S. Özdemir, V. Prokopiuk, V. Klochkov, N. Kavok, A. Onishchenko, P. Maksimchuk, D. Butov, K. Ocakoglu, Antimicrobial effects of nanostructured rare-earth-based orthovanadates, Curr. Microbiol. 79 (2022) 254. https://doi.org/10.1007/s00284-022-02947-w
16. Y.V. Nikitchenko, V.K. Klochkov, N.S. Kavok, N.A. Karpenko, S.L. Yefimova, I.V. Nikitchenko, A.I. Bozhkov, Age-related effects of orthovanadate nanoparticles involve activation of GSH-dependent antioxidant system in liver mitochondria, Biol. Trace Elem. Res. 199 (2021) 649–659. https://doi.org/10.1007/s12011-020-02241-0
17. Y.V. Nikitchenko, V.K. Klochkov, N.S. Kavok, K.A. Averchenko, N.A. Karpenko, I.V. Nikitchenko, S.L. Yefimova, A.I. Bozhkov, Anti-aging effects of antioxidant rare-earth orthovanadate nanoparticles in Wistar rats, Biol. Trace Elem. Res. 199 (2021) 4183–4192. https://doi.org/10.1007/s12011-020-02527-3
18. Y. Nikitchenko, V. Klochkov, N. Kavok, N. Karpenko, I. Nikitchenko, S. Yefimova, A. Bozhkov, Comparative studies of orthovanadate nanoparticles and metformin on life quality and survival of senile Wistar rats, Biol. Trace

Elem. Res. 200 (2022) 1237–1247. https://doi.org/10.1007/s12011-021-02707-0
19. J.M. Carvalho-Silva, A. Cândido dos Reis, Anti-inflammatory action of silver nanoparticles in vivo: Systematic review and meta-analysis, Heliyon 10 (2024) e34564. https://doi.org/10.1016/j.heliyon.2024.e34564
20. A. Luceri, R. Francese, D. Lembo, M. Ferraris, C. Balagna, Silver Nanoparticles: Review of antiviral properties, mechanism of action and applications, Microorganisms 11 (2023) 629. https://doi.org/10.3390/microorganisms11030629
21. V. Dhapte, S. Kadam, A. Moghe, V. Pokharkar, Probing the wound healing potential of biogenic silver nanoparticles, J. Wound Care 23 (2014) 431–436. https://doi.org/10.12968/jowc.2014.23.9.431
22. M. Rybka, L. Mazurek, Beneficial effect of wound dressings containing silver and silver nanoparticles in wound healing—from experimental studies to clinical practice, Life 13 (2023) 69. https://doi.org/10.3390/life13010069
23. A. Huignard, V. Buissette, A.C. Franville, T. Gacoin, J.P. Boilot, Emission processes in YVO_4:Eu nanoparticles, J. Phys. Chem. B 107 (2003) 6754–6759. https://doi.org/10.1021/jp0342226
24. V.K. Klochkov, A.I. Malyshenko, O.O. Sedyh, Y.V. Malyukin, Wet-chemical synthesis and characterization of luminescent colloidal nanoparticles: $ReVO_4$:Eu^{3+} (Re = La, Gd, Y) with rod-like and spindle-like shape, Funct. Mater. 1 (2011) 111–115.
25. G. Grygorova, V. Klochkov, O. Sedyh, Y. Malyukin, Aggregative stability of colloidal $ReVO_4$:Eu^{3+} (Re = La, Gd, Y) nanoparticles with different particle sizes, Colloids Surf. A 457 (2014) 495–501. https://doi.org/10.1016/j.colsurfa.2014.04.047
26. A. Loiseau, V. Asila, G. Boitel-Aullen, M. Lam, M. Salmain, S. Boujday, Silver-based plasmonic nanoparticles and their use in biosensing, Biosensors 9 (2019) 78. https://doi.org/10.3390/bios9020078
27. V. Klochkov, Comparative analysis of photocatalytic activity of aqueous colloidal solutions of $ReVO_4$:Eu^{3+} (Re = La, Gd, Y), $CePO_4$:Tb, CeO_2 and C_{60}, J. Photochem. Photobiol. A Chem. 310 (2015) 128–133. https://doi.org/10.1016/j.jphotochem.2015.04.005
28. S.L. Yefimova, P.O. Maksimchuk, K.A. Hubenko, V.K. Klochkov, I.A. Borovoy, A.V. Sorokin, Y.V. Malyukin, Untangling the mechanisms of $GdYVO_4$:Eu^{3+} nanoparticle photocatalytic activity, Colloids Surf. A 577 (2019) 630–636. https://doi.org/10.1016/j.colsurfa.2019.06.066
29. G. Pulido-Reyes, I. Rodea-Palomares, S. Das, T.S. Sakthivel, F. Leganes, R. Rosal, S. Seal, F. Fernandez-Pinas, Untangling the biological effects of cerium oxide nanoparticles: The role of surface valence states, Sci. Rep. 5 (2015) 15613. https://doi.org/10.1038/srep15613
30. Y. Li, W. Zhang, J. Niu, Y. Chen, Mechanism of photogenerated reactive oxygen species and correlation with the antibacterial properties of engineered metal-oxide nanoparticles, ACS Nano 6 (2012) 5164–5175. https://doi.org/10.1021/nn300934k
31. G. Rothenberger, J. Moser, M. Grätzel, K. Devendra, N. Serpone, D.K. Sharma, Charge carrier trapping and recombination dynamics in small semiconductor particles, J. Am. Chem. Soc. 107 (1985) 8054–8059. https://doi.org/10.1021/ja00312a043
32. M.L. de Souza, D.P. dos Santos, P. Corio, Localized surface plasmon resonance enhanced photocatalysis: an experimental and theoretical mechanistic investigation, RSC Adv. 8 (2018) 28753. https://doi.org/10.1039/c8ra03919d
33. T. Kong, A. Liao, Y. Xu, X. Qiao, H. Zhang, L. Zhang, C. Zhang, Recent advances and mechanism of plasmonic metal–semiconductor photocatalysis, RSC Adv. 14 (2024) 17041. https://doi.org/10.1039/d4ra02808b
34. L. Zhou, Q. Huang, Y. Xia, Plasmon-induced hot electrons in nanostructured materials: generation, collection, and application to photochemistry, Chem. Rev. 124 (2024) 8597–8619. https://doi.org/10.1021/acs.chemrev.4c00165
35. A. Loiseau, V. Asila, G. Boitel-Aullen, M. Lam, M. Salmain, S. Boujday, Silver-based plasmonic nanoparticles for and their use in biosensing, Biosensors 9 (2019) 78. https://doi.org/10.3390/bios9020078
36. A. Huignard, V. Buissette, A.C. Franville, T. Gacoin, J.P. Boilot, Emission processes in YVO_4:Eu nanoparticles, J. Phys. Chem. B 107 (2003) 6754–6759. https://doi.org/10.1021/jp0342226
37. M. Anitha, P. Ramakrishnan, A. Chatterjee, G. Alexander, H. Singh, Spectral properties and emission efficiencies of $GdVO_4$ phosphors, Appl. Phys. A 74 (2002) 153–162. https://doi.org/10.1007/s003390100981
38. K. Awazu, M. Fujimaki, C. Rockstuhl, J. Tominaga, H. Murakami, Y. Ohki, N. Yoshida, T. Watanabe, A plasmonic photocatalyst consisting of silver nanoparticles embedded in titanium dioxide, J. Am. Chem. Soc. 130 (2008) 1676–1680. https://doi.org/10.1021/ja076503